WILEY | Hindawi

Research Article

Robust Tracking Control of a Three-Phase Bidirectional Charger for Electric Vehicle

Chivon Choeung [iD],[1,2] Meng Leang Kry,[3] and Young-Il Lee [iD][4]

[1]*Faculty of Electricity, National Polytechnic Institute of Cambodia, Phnom Penh, Cambodia*
[2]*Graduate School, National Polytechnic Institute of Cambodia, Phnom Penh, Cambodia*
[3]*Business and Transmission Department, Electricity of Cambodia, Phnom Penh, Cambodia*
[4]*Department of Electrical and Information Engineering, Seoul National University of Science and Technology, Seoul, Republic of Korea*

Correspondence should be addressed to Chivon Choeung; choeungchivon@npic.edu.kh

This paper presents a robust control strategy for an electric vehicle's three-phase off-board bidirectional AC-DC battery charger. The conventional constant current (CC) and constant voltage (CV) charging mode are considered to provide a fast-charging performance for the batteries. The bidirectional charger also allows using of the vehicle as an energy storage system for the grid i.e., charging during the peak-off times and delivering the energy back to the grid during peak times of electrical consumption. In discharging mode, the bidirectional charger maintains constant active power flow to the grid with a given reference. For both cases, user of a robust state feedback controller with integral action is made in the *DQ*-synchronous frame. The set of stabilizing gains of this controller are determined by a linear matrix inequality (LMI)-based optimization so that the convergence time to steady stead is minimized in the occurrence of the parametric uncertainties of the L-filter. The efficacy of the proposed controller is verified through simulation and experimental results on 102.4 V Lithium iron phosphate (LiFePO$_4$) batteries.

1. Introduction

With a tremendous demand for renewable energy throughout the world, sustainable transportation methods draw a lot of attention in comparison to conventional transportation [1]. An enormous number of electric vehicles (EV) and plug-in hybrid electric vehicles (PHEV) are currently being utilized due to their eco-friendly behavior. For that reason, researchers, governments, and automakers worldwide continue to pursue efforts through policy and design to increase the EV market share. Many control techniques have been proposed to answer to the demands of rapid charging and energy-efficient battery charger.

In [1, 2] conventional proportional integral (PI) control has been studied for single-phase bidirectional chargers. These methods were proposed using a constant-current (CC) and a constant-voltage charging stage that produce faster-charging capability than that of only fixed voltage charging methods. The topology of these methods is single-phase based, so the amount of charging current of these chargers is less than those of the three-phase topology. Moreover, another main drawback of the PI controller of [1, 2] is to gain tuning efforts for both inner-loop and outer-loop controllers.

A bidirectional three-phase charger has been proposed using model predictive control [3]. This scheme provides a bidirectional power transfer with instantaneous mode charging capability and fast dynamic response. However, due to its only one charging stage (CV) from the grid to a vehicle (G2V), the batteries need more time to be fully charged. This method also requires a high computational power which results in high sampling frequency. Moreover, without integration of an integral control or a disturbance observer, this method may result in output offset-state error.

Deadbeat control has been presented in [4] for the DC-DC part of the bidirectional charger to regulate the charging

current to the battery while PI control is also used for the AC-DC converter side to maintain the DC-link voltage constant. It is known that deadbeat control produces fast transient performance in which settling time reaches the steady state in just a few sampling periods. This control method is sensitive to system uncertainty and measurement noise, particularly for high sampling frequency.

The topology of [1, 2], and [4] consist of a DC-DC converter for the CC/CV charging stage and an AC-DC converter for power factor and DC-link voltage control. In [5, 6], DC-DC converters have been used for single-phase chargers and [7, 8] for the three-phase charger to improve charging efficiency. Three operations of bidirectional chargers such as grid-to-vehicle (G2V), vehicle-to-grid (V2G), and vehicle-to-home (V2H) were considered in [5, 8] to provide a full charging capability of bidirectional charger for an electric vehicle. Yet, classical controllers such as PI and PR were adopted which results in multiloop gain tuning.

Taking battery lifespan into account, AI-based manufacturing and management have been reviewed in [9]. This review provides a systematic survey of AI-based manufacturing and management solutions for enhancing battery health performance with a focus on recent challenges and opportunities. Data science-based full-lifespan management strategies have also been discussed in [10] to furnish useful reference points to support the design of data science-based battery management solutions during its lifespan, while a brand-new hologram to make full use of battery during full-lifespan will be formulated.

In the case of advanced control methods, battery temperature is considered a key part of the battery thermal management for battery operation safety and behavior. In [11], a constrained generalized predictive control was proposed based on a newly developed coupled thermoelectric model. This method can be easily implemented in other battery charging applications to control the charge current and guarantee charging efficiency with a long lifespan. A leader-follower-based approach has been discussed in [12] to enable optimal charging control for the Li-ion battery pack. This method is capable of reducing the computational burden and enhancing the robustness to minimize the negative impact of the cells' model bias.

In this paper, a robust tracking control of a three-phase bidirectional charger is presented for electric vehicle applications without using a DC-DC converter as an interface between a three-phase AC-DC converter and batteries. The LMI-based robust tracking control is a well-known method and has been proposed for three-phase inverters [13, 14] and three-phase chargers [15, 16]. This proposed bidirectional charger is capable of charging Tesla Model S batteries which range between 352 V and 402 V. The battery is charged with a constant current until the voltage reaches the recommended maximum voltage, then the voltage is maintained constant until the current consumed by the battery falls to a residual value. During the discharging operation mode, the energy stored in the batteries can be delivered back to the power grid. The vehicle-to-grid (V2G) technology is crucial from the viewpoint of the European Union and the bidirectional charger allows to use of the Full Electric Vehicle as

an energy storage system for the electric grid, charging them in the peak-off times and delivering the energy back to the grid in peak times of electrical consume. For both cases, the use of a robust state feedback controller with integral action is made in the DQ-synchronous frame to provide stability and eliminate the steady-state error. Unlike a conventional MPC, this proposed controller is capable of removing an offset error to provide a good reference tracking output. This method also provides a systematic controller design by reducing the effort of gain tuning compared to the conventional PI controller and guaranteeing stabilized performance under parameter uncertainty. The set of stabilizing gains of this controller are determined by a linear matrix inequality (LMI)-based optimization so that the convergence time to steady stead is minimized in the occurrence of the parametric uncertainties of the L-filter. The consideration of an uncertainty model in this proposed method provides a wider range of good performance under the uncertain value of the L-filter than a deadbeat control. In the case of charging control, an outer-loop PI controller is employed to maintain the dc-current and dc-voltage for CC and CV control, respectively. The conventional phase-locked loop (PLL) is considered in this paper to obtain grid voltage phase angle.

2. System Description

A three-phase bidirectional charger circuit is shown in Figure 1. The dynamic of the line current is expressed in the abc-axis as follows:

$$\begin{cases} L\dfrac{di_a(t)}{dt} + Ri_a(t) = E_m \sin(\omega t) - v_{a,i} \\[2mm] L\dfrac{di_b(t)}{dt} + Ri_b(t) = E_m \sin\left(\omega t - \dfrac{2\pi}{3}\right) - v_{b,i}, \\[2mm] L\dfrac{di_c(t)}{dt} + Ri_c(t) = E_m \sin\left(\omega t - \dfrac{4\pi}{3}\right) - v_{c,i} \end{cases} \quad (1)$$

where

$$v_{a,i} := \frac{2u_a - u_b - u_c}{6v_o(t)},$$

$$v_{b,i} := \frac{-u_a + 2u_b - u_c}{6v_o(t)},$$

$$v_{c,i} := \frac{-u_a - u_b + 2u_c}{6v_o(t)}.$$

$$\text{Here,} \begin{cases} 1, & S_x = \text{on}; \quad \overline{S}_x = \text{off}; \\ & \quad\quad\quad\quad\quad\quad\quad\quad u_x\,(x = a, b, c). \\ -1, & S_x = \text{off}; \quad \overline{S}_x = \text{on}; \end{cases}$$

$$(2)$$

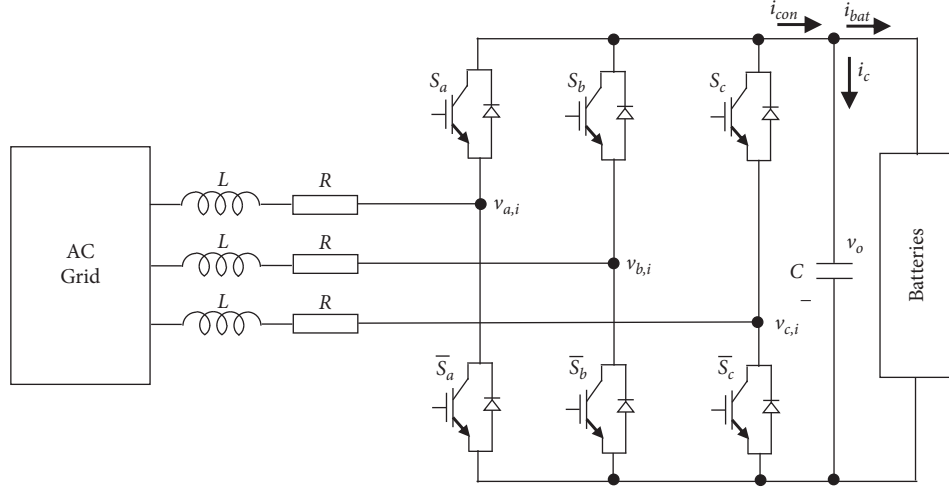The dynamic in abc-axis (1) can be transformed into the dq-axis as follows [17]:

FIGURE 1: Three-phase bidirectional charger with L-filter.

$$\frac{d\mathbf{i}_{dq}(t)}{dt} = \mathbf{A}_c \mathbf{i}_{dq}(t) + \mathbf{B}_c v_o(t)\mathbf{u}(t) + \mathbf{d}_c(t), \qquad (3)$$

where $\quad \mathbf{i}_{dq}(t) := \begin{bmatrix} i_d(t) \\ i_q(t) \end{bmatrix}, \quad \mathbf{u}(t) = \begin{bmatrix} u_d(t) \\ u_q(t) \end{bmatrix}, \quad \mathbf{d}_c(t) =$

$\begin{bmatrix} 0 \\ -E_m/L \end{bmatrix}, \mathbf{A}_c = \begin{bmatrix} -R/L & \omega \\ \omega & -R/L \end{bmatrix}, \mathbf{B}_c = \begin{bmatrix} -1/2L & 0 \\ 0 & -1/2L \end{bmatrix}$

ω is the angular frequency of the AC voltage source. The inductor current $\mathbf{i}_{dq}(t)$ and the control input $\mathbf{u}(t)$ in the dq-frame satisfy the relationship as follows:

$$\mathbf{i}_{dq}(t) = \frac{2}{3}\mathbf{T}(t)\mathbf{i}_{abc}(t), \mathbf{i}_{abc}(t) = \frac{3}{2}\mathbf{T}^T(t)\mathbf{i}_{dq}(t),$$

$$\mathbf{u}(t) = \frac{2}{3}\mathbf{T}(t)\mathbf{u}_{abc}(t), \mathbf{u}_{abc}(t) = \frac{3}{2}\mathbf{T}^T(t)\mathbf{u}(t),$$
$$(4)$$

where $\mathbf{T}(t) := \begin{bmatrix} \cos(\omega t) & \cos(\omega t + 2\pi/3) & \cos(\omega t + 2\pi/3) \\ -\sin(\omega t) & -\sin(\omega t + 2\pi/3) & -\sin(\omega t + 2\pi/3) \end{bmatrix}$,

$$\mathbf{T}^T(t) := \begin{bmatrix} \cos(\omega t) & -\sin(\omega t) \\ \cos\left(\omega t - \dfrac{2\pi}{3}\right) & -\sin\left(\omega t - \dfrac{2\pi}{3}\right) \\ \cos\left(\omega t - \dfrac{2\pi}{3}\right) & -\sin\left(\omega t - \dfrac{2\pi}{3}\right) \end{bmatrix}. \qquad (5)$$

On the other hand, the output voltage $v_o(t)$ in the state equation (2) is governed by the following dynamic:

$$C\frac{dv_o(t)}{dt} = i_{con.}(t) - i_{bat.}(t), \qquad (6)$$

where

$$i_{con.}(t) = \frac{3}{4}\mathbf{i}_{dq}^T(t)\mathbf{u}(t). \qquad (7)$$

where $i_{con.}$ is the converter current and $i_{bat.}$ is an output current to the battery.

The control input variable $\mathbf{u}(t) := \begin{bmatrix} u_d(t) & u_q(t) \end{bmatrix}^T$ must be constrained as follows [18]:

$$\|\mathbf{u}(t)\| \le \frac{2}{\sqrt{3}}. \qquad (8)$$

The dynamic (2) can be transformed in the following discrete time with sampling period h [19] as follows:

$$\mathbf{x}(k+1) = \mathbf{A}_d\mathbf{x}(k) + \mathbf{B}_d v_o(t)\mathbf{u}(k) + \mathbf{d}(k), \qquad (9)$$

where $\quad \mathbf{x}(k) := [i_d(k)/i_q(k)], \qquad \mathbf{A}_d = e^{\mathbf{A}_c h} =$

$e^{-\alpha h}\begin{bmatrix} \cos(\omega h) & \sin(\omega h) \\ -\sin(\omega h) & \cos(\omega h) \end{bmatrix}$, $\mathbf{d} = (\int_0^h e^{\mathbf{A}_c t}dt)\mathbf{d}_c = E_m/L\begin{bmatrix} b_1 \\ b_2 \end{bmatrix}$,

$\mathbf{B}_d = (\int_0^h e^{\mathbf{A}_c t}dt)\mathbf{B}_c = 1/2L\begin{bmatrix} b_1 & b_2 \\ -b_2 & b_1 \end{bmatrix}$, $\alpha := R/L$.

$$b_1 := \frac{\alpha - e^{-\alpha h}(\alpha \cos(\omega h) - \omega \sin(\omega h))}{\alpha^2 + \omega^2},$$
$$(10)$$
$$b_2 := \frac{\omega - e^{-\alpha h}(\omega \cos(\omega h) + \alpha \sin(\omega h))}{\alpha^2 + \omega^2}.$$

3. Model Uncertainties and Offset-free Control

In this section, the uncertainties model of the system and offset-free control are discussed. Suppose that the value of L and R in each phase are equal but vary in certain ranges below as follows:

$$L_{\min} \le L \le L_{\max}, \qquad (11a)$$

$$R_{\min} \le R \le R_{\max}. \qquad (11b)$$

Here, we denote the matrices $(\mathbf{A}_d, \mathbf{B}_d)$ corresponding to the four possible combinations of the immoderate value of $1/L$ and $1/R$ as $(\mathbf{A}_i, \mathbf{B}_i)$ $(i=1,2,3,4)$ and suppose that the matrices $(\mathbf{A}_d, \mathbf{B}_d)$ belong to the polytopic uncertain set $\mathbf{\Psi}$ below as follows:

$$\mathbf{\Psi} = \left\{ \sum_{n=1}^{4} \mu_n (\mathbf{A}_i, \mathbf{B}_i) \middle| \sum_{n=1}^{4} \mu_n = 1, \mu_n \ge 0 \right\}. \qquad (12)$$

The uncertainties of the system can be any kind of variation but should lie within the range (9). The system uncertain range can be determined as follows:

$$L_0/\mu \leq L \leq \mu L_0, \tag{13a}$$

$$R_0/\mu \leq R \leq \mu R_0, \tag{13b}$$

where R_0 and L_0 are the nominal value of the filter resistance and inductance, respectively, and μ (>1) can be considered as a tuning parameter.

To compensate for the offset error despite the system's uncertainty model, the control law based on [10] is employed for (8) as follows:

$$\begin{cases} \mathbf{w}(k) = \mathbf{w}(k+1) + (\mathbf{x}_{\text{ref}} - \mathbf{x}(k-1)) \\ \mathbf{u}(k) = \mathbf{Kx}(k) + \mathbf{Lw}(k) \end{cases}, \tag{14}$$

where $\mathbf{K}$ and $\mathbf{L}$ are state feedback and integrator gains, respectively. Because of the integrator in (12), the steady-state error between the reference state $\mathbf{x}_{ref}$ and the grid-current $\mathbf{x}$ will be compensated provided that the closed-loop system is stable. The reference state $\mathbf{x}_{\text{ref}} := \begin{bmatrix} i_{\text{d}}^{\text{ref}} & i_q^{\text{ref}} \end{bmatrix}^T$ is generated by the outer-loop controller in the case of charging mode and can be computed with a given power reference in the case of discharging stage.

4. Robust Optimal Gain

Here, let us determine the gains of (12) so that the closed-loop stability is provided to the system in the occurrence of parametric uncertainties. A systematic design method is proposed to obtain stabilizing state feedback gain $\mathbf{K}$ and integral gain $\mathbf{L}$ using LMI. From relations (8) and (12), we get the following:

$$\begin{bmatrix} \mathbf{x}(k+1) \\ \mathbf{w}(k+1) \end{bmatrix} = \begin{bmatrix} \mathbf{A}_d & \mathbf{0}_{2\times 2} \\ -\mathbf{C} & \mathbf{I}_{2\times 2} \end{bmatrix} \begin{bmatrix} \mathbf{x}(k) \\ \mathbf{w}(k) \end{bmatrix} + \begin{bmatrix} \mathbf{B}_d \\ \mathbf{0}_{2\times 1} \end{bmatrix} \mathbf{u}(k) + \begin{bmatrix} \mathbf{d}(k) \\ \mathbf{x}_{ref} \end{bmatrix}. \tag{15}$$

where output matrix $\mathbf{C} = \begin{bmatrix} 1 & 0 \\ 0 & 1 \end{bmatrix}$. Relation (13) can be simplified as follows:

$$\overline{x}(k+1) = \mathbf{A}_u \overline{x}(k) + \mathbf{B}_u \mathbf{u}(k) + \mathbf{D}(k), \tag{16}$$

where $\overline{x}(k) := \begin{bmatrix} \mathbf{x}(k) \\ \mathbf{w}(k) \end{bmatrix}$, $\mathbf{A}_u := \begin{bmatrix} \mathbf{A}_u & \mathbf{0}_{2\times 2} \\ -\mathbf{C} & \mathbf{I}_{2\times 2} \end{bmatrix}$, $\mathbf{B}_u := \begin{bmatrix} \mathbf{B}_d \\ \mathbf{0}_{2\times 2} \end{bmatrix}$, $\mathbf{D}(k) := \begin{bmatrix} \mathbf{d}(k) \\ \mathbf{x}_{ref} \end{bmatrix}$.

The control input $\mathbf{u}(k)$ can be given as follows:

$$\mathbf{u}(k) = \mathbf{F}\overline{x}(k)\mathbf{F} := \begin{bmatrix} \mathbf{K} & \mathbf{L} \end{bmatrix}. \tag{17}$$

Suppose that $\mathbf{D}(k) = 0$ to determine stabilizing gain $\mathbf{F}$, then the closed-loop system can be computed as follows:

$$\overline{x}(k+1) = (\mathbf{A}_u + \mathbf{B}_u \mathbf{F})\overline{x}(k). \tag{18}$$

The closed-loop system (16) is stable [20] if there exists a positive-definite matrix $\mathbf{W}$ such that

$$\mathbf{W} - (\mathbf{A}_u + \mathbf{B}_u \mathbf{F})^T \mathbf{W} (\mathbf{A}_u + \mathbf{B}_u \mathbf{F}) > 0. \tag{19}$$

It can be seen that the condition (17) holds for some $\mathbf{W}_0 > 0 \, (\mathbf{W}_0 < \mathbf{W})$

$$\mathbf{W}_0 - (\mathbf{A}_u + \mathbf{B}_u \mathbf{F})^T \mathbf{W} (\mathbf{A}_u + \mathbf{B}_u \mathbf{F}) > 0. \tag{20}$$

By employing Schur complement [20] to (18), we get

$$\begin{bmatrix} \mathbf{S}_0 & (\mathbf{A}_u \mathbf{S}_0 + \mathbf{B}_u \mathbf{H})^T \\ \mathbf{A}_u \mathbf{S}_0 + \mathbf{B}_u \mathbf{H} & \mathbf{S} \end{bmatrix} > 0, \tag{21}$$

where $\mathbf{H} := \mathbf{FS}_0$, $\mathbf{S} := \mathbf{W}^{-1}$ and $\mathbf{S}_0 := \mathbf{S}_0^{-1}$. It should be noted that the matrices $\mathbf{A}_u$ and $\mathbf{B}_u$ contain the uncertain matrices $\mathbf{A}_d$ and $\mathbf{B}_d$; thus, (19) should hold for all $(\mathbf{A}_d, \mathbf{B}_d) \in \Psi$. To ensure that (19) is met for all $(\mathbf{A}_d, \mathbf{B}_d) \in \Psi$, we should verify that the condition is satisfied at all corners of the set Ψ i.e.,

$$\begin{bmatrix} \mathbf{S}_0 & \mathbf{S}^T \mathbf{A}_{ui}^T + \mathbf{H}^T \mathbf{B}_{ui}^T \\ \mathbf{A}_{ui} \mathbf{S}_0 + \mathbf{B}_{ui} \mathbf{H} & \mathbf{S} \end{bmatrix} > 0, \, (i = 1, 2, 3, 4), \tag{22}$$

where $\mathbf{A}_{ui} := \begin{bmatrix} \mathbf{A}_i & \mathbf{0}_{2\times 2} \\ -\mathbf{C} & \mathbf{I}_{2\times 2} \end{bmatrix}$, $\mathbf{B}_{ui} := \begin{bmatrix} \mathbf{B}_i \\ \mathbf{0}_{2\times 2} \end{bmatrix}$, $(i = 1, 2, 3, 4)$.

Summarizing the above discussion, a closed-loop system (16) is asymptotically stable if there exist symmetric positive definite matrices $\mathbf{S}$, $\mathbf{S}_0$ and a matrix $\mathbf{H}$ such that (20) holds, and the stabilizing gain is given as follows:

$$\mathbf{F} = \mathbf{HS}_0^{-1}. \tag{23}$$

Suppose that $\mathbf{W}_0 < \alpha \mathbf{W}$ or

$$\mathbf{S} < \alpha \mathbf{S}_0 \, (0 < \alpha < 1). \tag{24}$$

Then, (18) implies that for $k > 0$,

$$\overline{x}^T(k) (\mathbf{A}_a + \mathbf{B}_a \mathbf{F})^T \mathbf{W} (\mathbf{A}_a + \mathbf{B}_a \mathbf{F})\overline{x}(k),$$
$$= \overline{x}^T(k+1)\mathbf{W}\overline{x}(k+1) < \overline{x}^T(k)\mathbf{W}_0\overline{x}(k) < \alpha \overline{x}^T(k)\mathbf{W}\overline{x}(k). \tag{25}$$

It can be expected that a small α would give a fast convergence of $\mathbf{z}$ to the origin. Therefore, to obtain optimal gain $\mathbf{F}$ such that the convergence time is minimized, the following optimization problem should be solved.

$$\underset{\substack{\mathbf{S}, \mathbf{S}_0 > 0, \\ \alpha > 0, \mathbf{H}}}{\text{Minimize}} \quad \alpha \text{ subject to } (20) \text{ and } (22). \tag{26}$$

This optimization scheme is a generalized eigenvalue problem that can be solved efficiently by MATLAB Toolbox. The convergence of this control method can be found in [20].

It can be noted that the controller with optimal gain $\mathbf{F}$ determined by solving problem (23) satisfies the condition (17) and guarantees the overall closed-loop stability for any of the variations on the filter's inductance L and resistance R as long as it stays within the uncertain range (9).
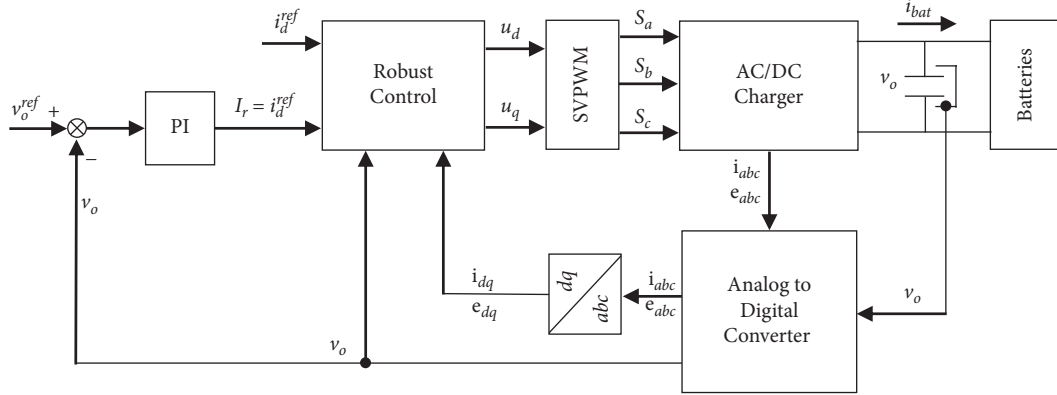
FIGURE 2: Block diagram of CV mode control.

5. Outer-Loop Charging Control

To perform the battery charging process, most of the battery manufacturers recommend two charging stages: constant current (CC) followed by constant voltage (CV). The battery is charged with a constant current until the voltage reaches the recommended maximum voltage, then the voltage is maintained constant until the current consumed by the battery falls to a residual value. The control of these two charging states is discussed in this section.

5.1. Constant Voltage (CV) Charging Mode.
Here, the outer-loop PI control for constant voltage charging is discussed. Suppose that the dynamics of the inner-loop control in the previous section are considerably fast so that we could assume.

$$i_{\text{con.}}(t) \approx I_r(t), \tag{27}$$

for some current reference $I_r(t)$. Let I_r be the output of the outer-loop control, i.e.,

$$I_r(t) = K_p\left(v_o^{\text{ref}} - v_o(t)\right) + K_i \int v_o^{\text{ref}} - v_o(t)\mathrm{dt}, \tag{28}$$

where v_o^{ref} is the constant voltage reference and $v_o(t)$ is the output voltage. From (5) and (25), we get

$$C\frac{dv_o(t)}{dt} + K_p\left(v_o^{\text{ref}} - v_o(t)\right) + K_i \int \left(v_o^{\text{ref}} - v_o(t)\right)dt - i_{\text{bat.}}(t). \tag{29}$$

or

$$C\frac{d^2v_o(t)}{dt} = K_p\frac{dv_o(t)}{dt} + K_i v_o(t) = K_i v_o^{\text{ref}}. \tag{30}$$

The K_i and K_p gain can be determined by considering the characteristic polynomial of (27) and can be given as follows:

$$\Delta(s) = s^2 + 2\zeta\omega_r s + \omega_r^2. \tag{31}$$

for some appropriate value of ζ and ω_r^2; we get

$$\begin{aligned}
K_i &= \omega_r^2, \\
K_p &= 2\zeta\omega_r.
\end{aligned} \tag{32}$$

The control diagram of the constant voltage control of the three-phase bidirectional charger is shown in Figure 2. The battery voltage is fed-back to the out-loop controller, which produces a reference current $i_r = i_q^{ref}$. A conventional phase-locked loop (PLL) is used in the controller to obtain the phase-angle of the grid voltage.

5.2. Constant Current (CC) Charging Mode.
In the constant current charging stage, the battery pack is charged with a fixed current until the voltage reaches the recommended maximum voltage, then switch to the constant voltage charging stage. For the control of this constant current charging mode, an outer-loop PI is utilized to generate a reference signal $i_r = i_q^{\text{ref}}$ for inner-loop robust control with the same concept as CV charging discussed in the previous section. The control structure of the proposed CC charging control is validated as shown in Figure 3.

The control structure of both CC and CV charging modes are almost identical, however, the main difference is the use of outer-loop feedback; i_{bat} and v_o for CC and CV charging modes, respectively.

6. Discharging Control

Unlike CC and CV, this control scheme does not require the outer-loop controller; however, an uncomplicated computation of the reference state $\mathbf{x}_{ref}$ is needed. The discharging controller allows the battery charger delivers constant power back to the grid with a given reference P_{ref}.

Now, let us consider how to compute the reference state $\mathbf{x}_{ref}$ for the proposed robust controller. The instantaneous active and reactive power can be represented in the $\alpha\beta$-frame [21] as follows:

$$\begin{bmatrix} P_o \\ Q_o \end{bmatrix} = \frac{3}{2}\begin{bmatrix} e_\alpha & e_\beta \\ e_\beta & -e_\alpha \end{bmatrix}\begin{bmatrix} i_\alpha \\ i_\beta \end{bmatrix}, \tag{33}$$

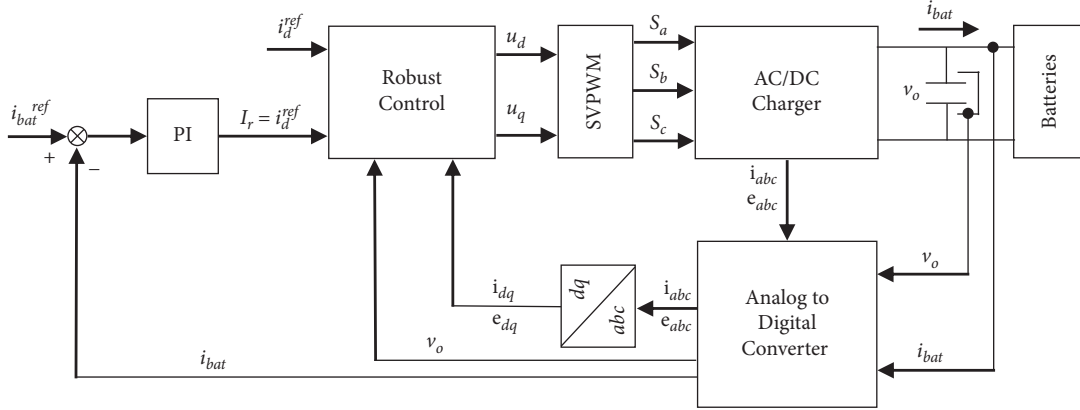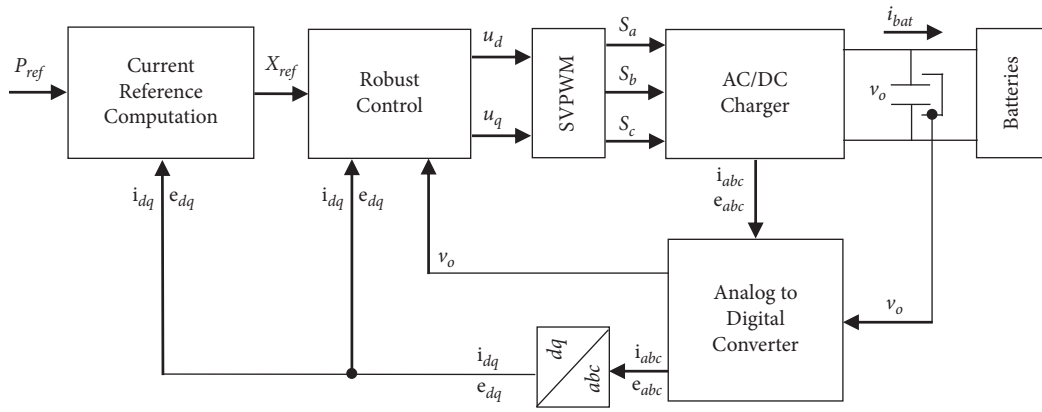Figure 3: Block diagram of CC mode control.

Figure 4: Block diagram of discharging mode control.

where $i_{\alpha\beta}$, $e_{\alpha\beta}$, P_o, and Q_o are grid-current in $\alpha\beta$-frame, grid-voltage in $\alpha\beta$-frame, grid active power and grid reactive power, respectively. Then, the relation (31) can be transformed to dq-frame as follows:

$$\begin{bmatrix} P_o \\ Q_o \end{bmatrix} = \frac{3}{2} \begin{bmatrix} e_d & e_q \\ -e_q & e_d \end{bmatrix} \begin{bmatrix} i_d \\ i_q \end{bmatrix}. \tag{34}$$

i_{dq} and e_{dq} are grid-current and voltage in dq-frame, respectively. From (32), the grid-current can be computed as follows:

$$\begin{bmatrix} i_d \\ i_q \end{bmatrix} = \frac{2}{3} \begin{bmatrix} e_d & e_q \\ -e_q & e_d \end{bmatrix}^{-1} \begin{bmatrix} P_o \\ Q_o \end{bmatrix}. \tag{35}$$

or

$$\begin{bmatrix} i_d^{\mathrm{ref}} \\ i_q^{\mathrm{ref}} \end{bmatrix} = \frac{2}{3} \begin{bmatrix} e_d & e_q \\ -e_q & e_d \end{bmatrix}^{-1} \begin{bmatrix} P_{\mathrm{ref}} \\ Q_{\mathrm{ref}} \end{bmatrix}. \tag{36}$$

In order to maintain a unity power factor, reactive power should be eliminated, and the reference can be computed as follows:

Table 1: Simulation parameters.

Parameters	Value
Grid phase-voltage	60 V
DC-link capacitor	4700 μF
Filter resistance	0.1 Ω
Filter inductance	5 mH
Sampling rate	10 kHz
Constant current reference	5 A
Constant voltage reference	107 V

$$\mathbf{x}_{\mathrm{ref}} := \begin{bmatrix} i_d^{\mathrm{ref}} \\ i_q^{\mathrm{ref}} \end{bmatrix} = \frac{2P_{\mathrm{ref}}}{3M} \begin{bmatrix} e_d \\ e_q \end{bmatrix}, \tag{37}$$

where $M = e_d^2 + e_q^2$. The reference state $\mathbf{x}_{\mathrm{ref}}$ allows the charger to deliver constant power back to the grid with a given reference P_{ref}.

It can be noted that a negative power reference P_{ref} results in reverse current flowing, in another word current flow from batteries to the grid. We can charge the batteries with constant power by the positive P_{ref}. Moreover, the active and reactive power can be regulated directly by adjusting P_{ref} and Q_{ref} in (34), then the reference state can be obtained. The control structure of the proposed discharging control is validated as shown in Figure 4.
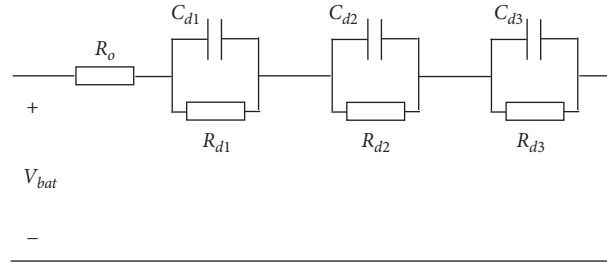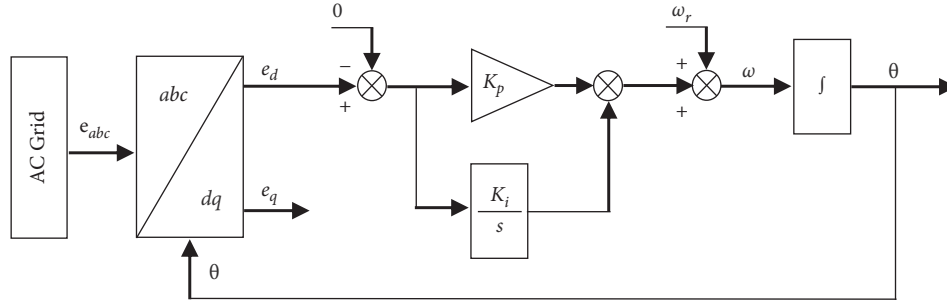
FIGURE 5: Battery equivalent circuit.

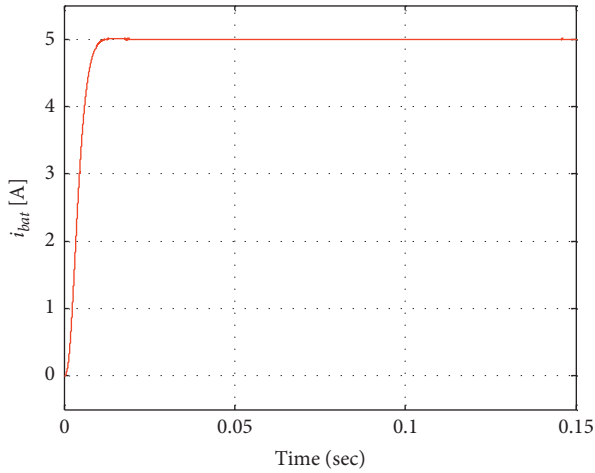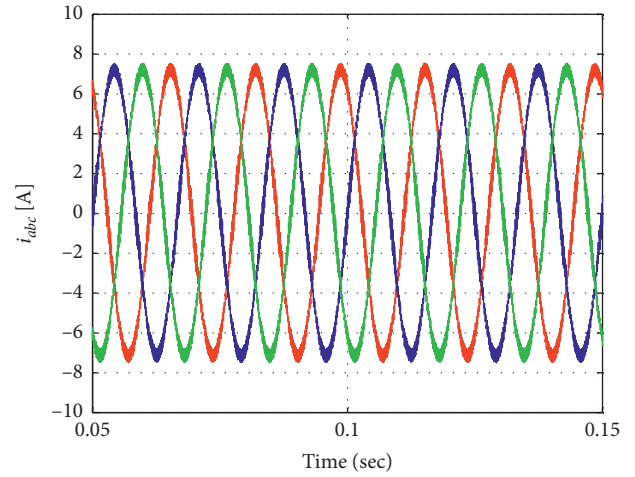FIGURE 6: Structure of conventional phase-locked loop.

FIGURE 7: Transient response of output current in CC mode.

- i_a
- i_b
- i_c

FIGURE 8: Steady-state grid current in CC mode.

7. Simulation Results

This section presents the results of the simulation on a three-phase AC/DC bidirectional charger to verify the efficacy of the proposed method. The simulation is implemented using the PSIM simulation tool and MATLAB LMI toolbox to obtain robust gain for the inner-loop controller. The parameters of the system are shown in Table 1. The control algorithm is conducted using a DLL block from Microsoft Visual Studio and the sampling rate is set to 10 kHz. An equivalent circuit in Figure 5 is used for the simulation studies.

The implementation of the proposed control strategy can be summarized as follows:

Step 1: Derive the discrete-time model based on (8) using the nominal value of inductance L and resistance R.

Step 2: Choose an initial uncertainty range of the parameters (11), e.g., $\mu = 1.1$, and corresponding set $\mathbf{\Psi}$.

Step 3: Compute the state feedback gain $\mathbf{K}$ and integrator gain $\mathbf{L}$ by solving the optimization problem (23).
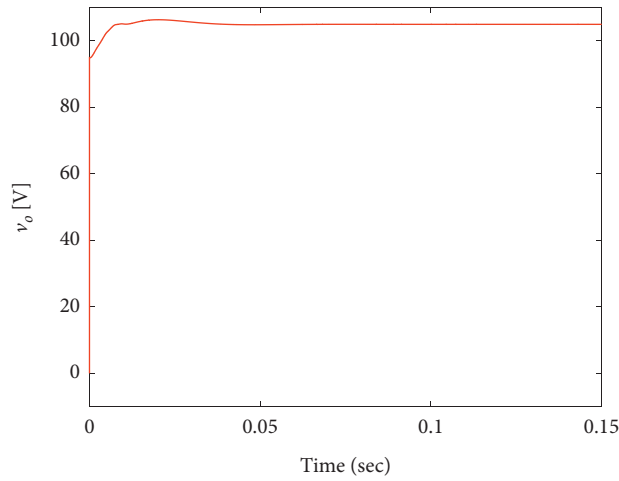
Step 4: Implement the control (12) to the charger.
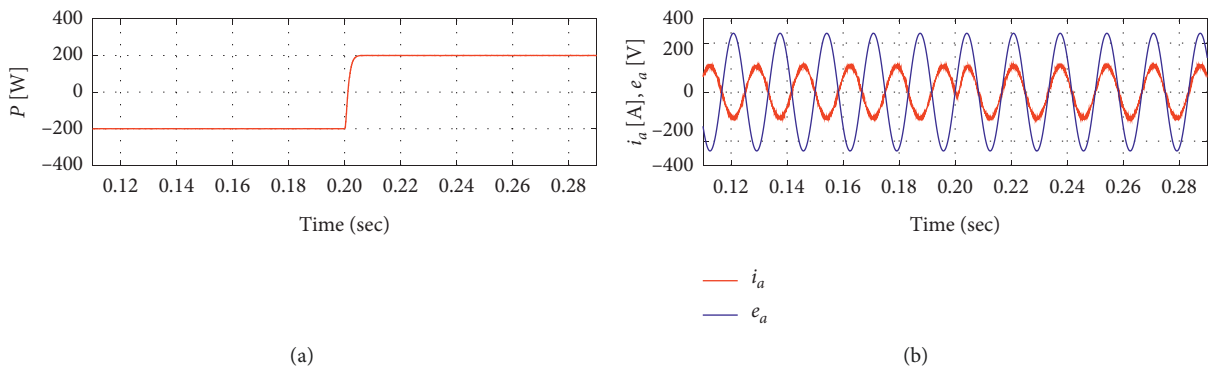
FIGURE 9: Transient response of output voltage in CV mode.

(a)

i_a

e_a

(b)

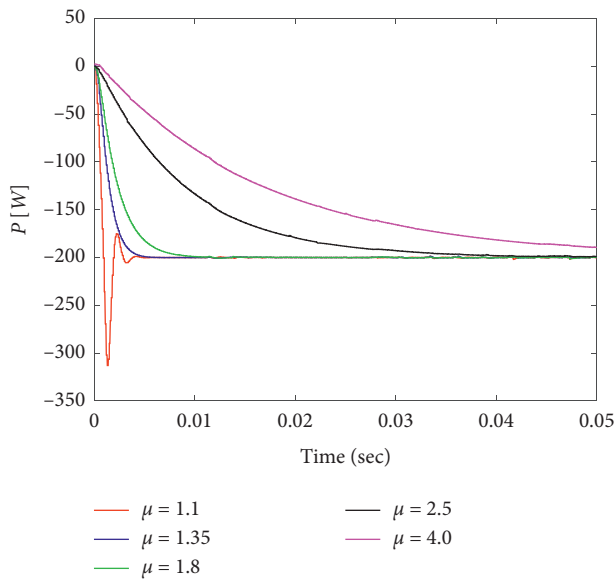FIGURE 10: (a) Active power and (b) grid voltage and current during discharging and charging mode.

$\mu = 1.1$ $\mu = 2.5$

$\mu = 1.35$ $\mu = 4.0$

$\mu = 1.8$

FIGURE 11: Active power using different uncertainties range μ in discharging mode.

FIGURE 12: Lithium iron phosphate (LiFePO4) battery pack.

Step 5: If the closed-loop system shows serious over-shoot or becomes unstable, then adjust the uncertainty range, i.e., raise the value of μ and repeat the procedure from Step 3.

Step 6: After the closed-loop system becomes stable, then apply the outer-loop control for CC or CV.

In this paper, a synchronous reference frame phase-locked loop (PLL) is used to estimate the frequency and phase angle of the grid voltage [22]. The control structure of the conventional PLL is shown in Figure 6.
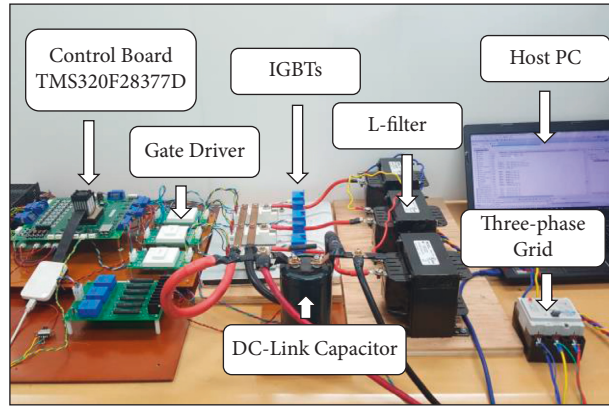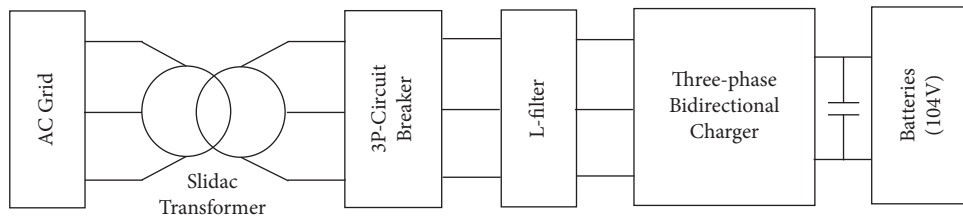
FIGURE 13: Experimental setups.

FIGURE 14: A simplified experimental setup circuit.

TABLE 2: Parameters of the prototype.

Parameters	Value
Grid phase-voltage	60 V (max)
DC-link capacitor	4700 μF
Filter resistance	0.2 Ω
Filter inductance	5 mH
Sampling rate	10 kHz
Constant current reference	5 A
Constant voltage reference	107 V
Battery (LiFePO$_4$)	102.4 V (20 Ah)

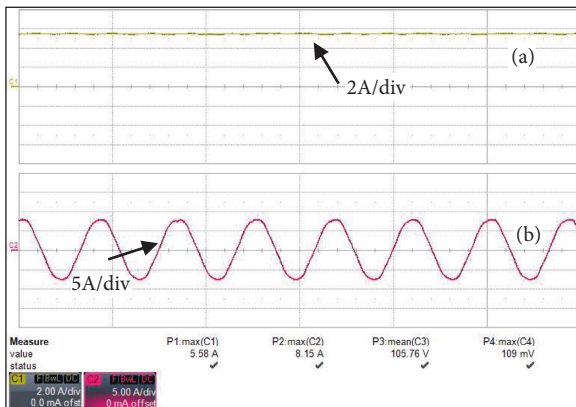FIGURE 15: Experimental results of (a) battery current and (b) phase-A grid current in CC mode.

FIGURE 16: Experimental results of three-phase grid-current in CC mode.

Here, the simulation performances of the proposed bidirectional charger are discussed. The transient response of the output current to the battery in CC mode is shown in Figure 7. T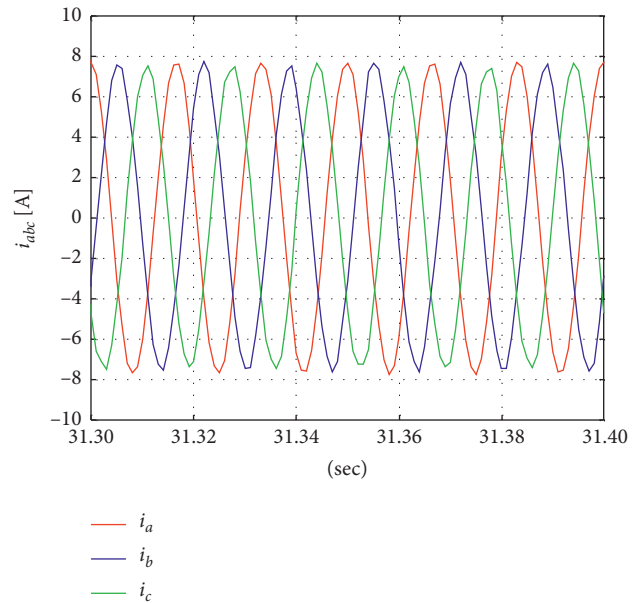his is the first charging stage of the batteries followed by constant voltage (CV) charging mode. We can see that the proposed robust control provides a fast-transient performance and smooth output current. The steady-state performance of the three-phase grid current is validated in Figure 8.

Figure 9 shows the transient performance of the output voltage in constant voltage CV charging mode. The bidirectional charger switches to this stage when the battery's voltage reaches a certain point after constant current CC charging mode. The outer-loop voltage control generates the
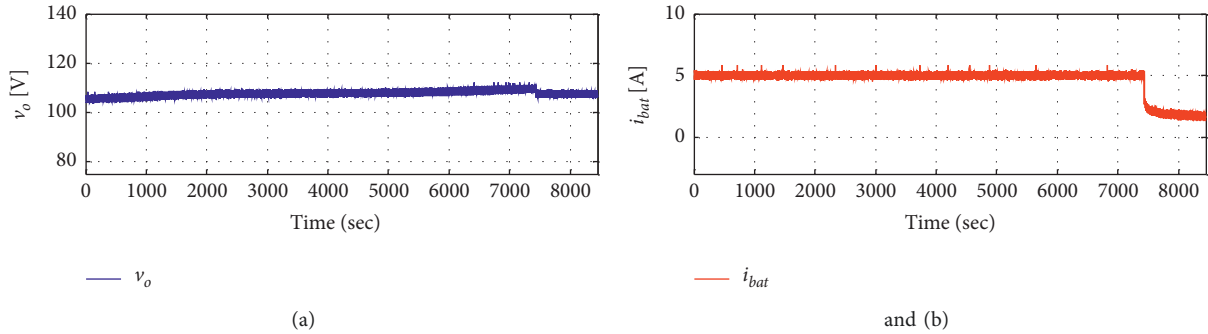
Figure 17: Experimental results of (a) battery voltage and (b) battery current in CC/CV.
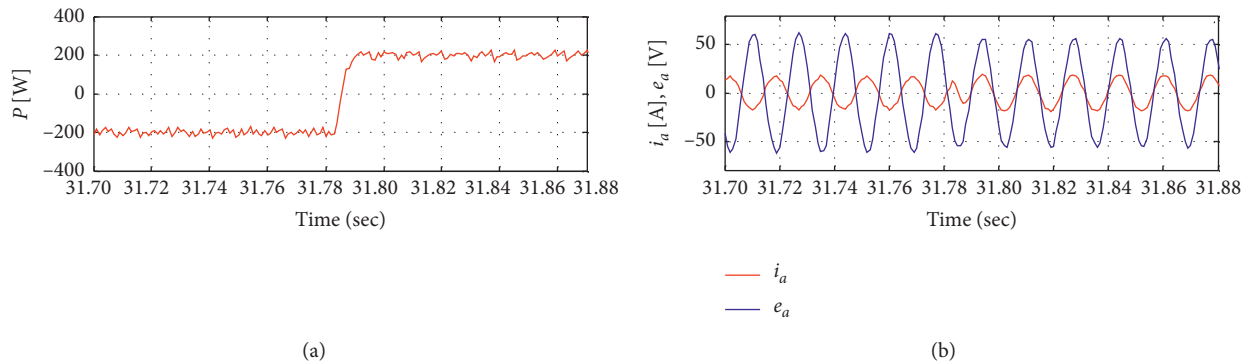

Figure 18: Experimental results of (a) active power and (b) grid-voltage and current during discharging and charging mode.

reference to inner-loop control (12) as shown in Figure 2. It can be seen that the output voltage to batteries is considerably fine.

For the simulation study in Figure 10(a), the discharging and charging of batteries with constant active power is validated. The battery is discharged with 200 W power at $t = 0.11$ s then switch to charging at $t = 0.29$ s with 200 W. It can be seen that the settling time to steady-state for both points is considerably fast and with smooth output power. Figure 10(b) shows phase-A grid voltage and current. We can see that the voltage and current are in $180°$ phase difference in discharging stage and change to in-phase during the charging period. It can be noted that all the aforementioned simulation results were carried out using the same uncertainty range ($\mu = 1.35$) because within this range we can obtain fast performance and no overshoot.

From Figure 11, a further study of using different uncertainty ranges is shown. The different selection of $\mu = (1.1, 1.35, 1.8, 2.5,$ and $4.0)$ in the equations (11a) and (11b) was made. From the figure, we can conclude that the use of $\mu = 1.1$ results in overshoot performance while sluggish performances are obtained with $\mu = 2.5$ and 4.0. Thus, a choice of μ between 1.35 and 1.8 would be considerable.

8. Experimental Results

For the experiment, a three-phase AC/DC converter with L-filter is used to charge 102.4 V Lithium iron phosphate (LiFePO$_4$) batteries. The proposed robust control was implemented on the TMS320F28377D digital signal processor with a sampling rate of 10 kHz. The battery packs consist of 64 cells, and the 32 pairs are connected in series. The actual battery pack is shown in Figure 12. A slide transformer is used to drop the grid voltage to a proper level to charge 102.4 V battery packs and the experimental setup is shown in Figure 13. A simplified experimental setup circuit is provided in Figure 14. The parameters of the experimental prototype are shown in Table 2.

Figure 15 shows experimental performances of battery charging current (a) and the phase-A grid-current (b) in steady stead with the reference current 5 A. It can be seen that the bidirectional charger can provide a smooth constant charging current to the batteries. Note that all the experimental data below is obtained by CAN communication from the control board.

In Figure 16, the steady state three-phase grid-current in charging mode is validated. We can see that a considerable balanced sinusoidal grid-current is obtained using this proposed control.

Figure 17 shows a full process of charging using CC and followed by CV. The battery is charged with constant 5 A until $t = 7400$ s then switched to constant voltage mode. From the figure, we can observe that the battery voltage is increasing to maintain a constant current. However, during the constant voltage charging stage, the battery current is dropping as time goes on.

For the experimental results in Figure 18(a), the discharging and charging of batteries with constant active power

power is shown. The battery is discharged with constant power, 200 W, then switch to the charging stage with 200 W. We can see that the settling time to steady-state for both points is considerably fast. Figure 18(b) shows a three-phase grid-current in discharging mode followed by charging mode. In both discharge and charging cases, an almost unity power can be obtained.

9. Conclusions

This paper describes a robust control strategy for a three-phase off-board bidirectional charger for an electric vehicle without using a DC-DC converter as an interface between a three-phase AC-DC converter and batteries. The conventional constant current (CC) and constant voltage (CV) charging mode are considered to provide a fast-charging performance for the batteries. The bidirectional charger also allows using of the electric vehicle as an energy storage system for the power grid. The proposed control consists of inner-loop robust control and outer-loop conventional PI control. For the inner-loop robust control, a state feedback controller with integral action is employed in dq-synchronous frame. The set of stabilizing gains of this controller are determined by an LMI-based optimization so that the convergence time to steady stead is minimized in the occurrence of the parametric uncertainties of the L-filter. It can be noted that the uncertainty range of the inductance and resistance can be considered a design parameter. Thus, its choice should be made depending on the resulting performances. From the simulation and experimental results, we can see that the proposed control for the bidirectional charger has considerable performance in both charging and discharging modes. The shortcoming of this proposed charger is that it is not capable of charging low voltage batteries due to the lack of a DC-DC converter as an interlink between the batteries and an AC-DC converter. The additional implementation of disturbance and state observers will be included in the future work of this research.

Abbreviations

CAN: Controller area network
CC: Constant current
CV: Constant voltage
EV: Electric vehicle
G2V: Grid to vehicle
LMI: Linear matrix inequality
PHEV: Plug-in hybrid electric vehicle
PI: Proportional integral
PLL: Phase-locked loop
PR: Proportional resonant
V2G: Vehicle-to-grid
V2H: Vehicle-to-home
L: Inductive filter
R: Filter resistance
C: Capacitive filter
$v_o(t)$:   Output voltage
S_{abc}:   Switching vector in abc-frame
$\mathbf{i}_{abc}(t)$:   Grid current vector in abc-frame
$\mathbf{i}_{\alpha\beta}(t)$:   Grid current vector in $\alpha\beta$-frame
$\mathbf{i}_{dq}(t)$:   Grid current vector in dq-frame
$\mathbf{u}(t)$:   Continuous time control input
E_m: Grid voltage magnitude
ω: Angular frequency
$i_{con.}$:   Converter current
$i_{bat.}$:   Battery current
$\mathbf{x}(k)$:   Discrete-time state
$\mathbf{u}(k)$:   Discrete-time control input
$L_{\min}$:   Lower bounce filter inductance
$L_{\max}$:   Upper bounce filter inductance
$R_{\min}$:   Lower bounce filter resistance
$R_{\max}$:   Upper bounce filter resistance
$\boldsymbol{\Psi}$:   Uncertainty set
μ: Uncertainty range
$\mathbf{w}(k)$:   Integral state
$\mathbf{L}$:   Integral gain
$\mathbf{K}$:   State feedback gain
$\mathbf{x}_{ref}$:   Reference state
$\mathbf{W}$:   Weighting matrix
$\overline{x}(k)$:   Augmented state
K_i: Outer loop integral gain
K_p: Outer loop proportional gain
P_o: Output active power
Q_o: Output reactive power
$\mathbf{e}_{\alpha\beta}$:   Grid voltage vector in $\alpha\beta$-frame
$\mathbf{e}_{dq}(t)$:   Grid voltage vector in dq-frame
P_{ref}:   Active power reference
Q_{ref}:   Reactive power reference.

Data Availability

The data used to support the findings of this study are available from the corresponding author upon reasonable request.

Conflicts of Interest

The authors declare that they have no conflicts of interest.

Acknowledgments

References

[1] J. G. Pinto, V. Monteiro, H. Goncalves et al., "Bidirectional battery charger with grid-to-vehicle, vehicle-to-grid and vehicle-to-home technologies," in *Proceedings of the 39th Annu. IEEE IECON*, pp. 5770–5775, Vienna, Austria, November 2013.

[2] X. Zhou, G. Wang, S. Lukic, S. Bhattacharya, and A. Huang, "Multi-Function Bi-directional Battery Charger for Plug-In Hybrid Electric Vehicle Application," in *Proceedings of the IEEE ECCE*, pp. 3930–3936, San Jose, CA, USA, 2009.

[3] M. Parvez, S. Mekhilef, N. M. L. Tan, and H. Akagi, "Model Predictive Control of a Bidirectional AC-DC Converter for V2G and G2V Applications in Electric Vehicle Battery Charger," in *Proceedings of the IEEE ITEC*, Dearborn, MI, USA, 2014.

[4] J. Gallardo-Lozano, M. I. Milanes-Montero, M. A. Guerrero-Martínez, and E. Romero-Cadaval, "Electric vehicle battery charger for smart grids," *Electric Power Systems Research*, vol. 90, pp. 18–29, 2012.

[5] M. Kwon and S. Choi, "An electrolytic capacitorless bidirectional EV charger for V2G and V2H applications," *IEEE Transactions on Power Electronics*, vol. 32, no. 9, pp. 6792–6799, 2017.

[6] U. K. T. Wajahat, M. Saad, and N. Mutsuo, "A transformerless reduced switch counts three-phase APF-assisted smart EV charger," in *Proceedings of the IEEE APEC*, Tampa, FL, USA, 2017.

[7] X. Wang, C. Jiang, B. Lei, H. Teng, H. K. Bai, and J. L. Kirtley, "Power-loss analysis and efficiency maximization of a silicon-carbide MOSFET-based three-phase 10-kW bidirectional EV charger using variable-DC-bus control," *IEEE Journal of Emerging and Selected Topics in Power Electronics*, vol. 4, no. 3, pp. 880–892, 2016.

[8] K. W. Hu, P. H. Yi, and C. M. Liaw, "An EV SRM drive powered by battery/supercapacitor with G2V and V2H/V2G capabilities," *IEEE Transactions on Industrial Electronics*, vol. 62, no. 8, pp. 4714–4727, 2015.

[9] K. Liu, Z. Wei, C. Zhang, Y. Shang, R. Teodorescu, and Q.-L. Han, "Towards long lifetime battery: AI-based manufacturing and management," *IEEE/CAA Journal of Automatica Sinica*, vol. 9, no. 7, pp. 1139–1165, 2022.

[10] K. Liu, Y. Wang, and X. Lai, *Data Science-Based Full-Lifespan Management of Lithium-Ion Battery: Manufacturing*, Operation, and Reutilization, 2022.

[11] K. Liu, K. Li, and C. Zhang, "Constrained generalized predictive control of battery charging process based on a coupled thermoelectric model," *Journal of Power Sources*, vol. 347, pp. 145–158, 2017.

[12] Q. Ouyang, Z. Wang, K. Liu, G. Xu, and Y. Li, "Optimal charging control for lithium-ion battery packs: a distributed average tracking approach," *IEEE Transactions on Industrial Informatics*, vol. 16, no. 5, pp. 3430–3438, May 2020.

[13] C. Choeung, S. H. Park, B. K. Koh, and Y. I. Lee, "Robust tracking control of a three-phase DC-AC inverter for UPS application under unbalanced load conditions," *IFAC-PapersOnLine*, vol. 49, no. 27, pp. 278–283, 2016.

[14] J. S. Lim, C. R. Park, J. H. Han, and Y. I. Lee, "Robust tracking control of a three-phase DC-AC inverter for UPS applications," *IEEE Transactions on Industrial Electronics*, vol. 61, no. 8, pp. 4142–4151, Aug. 2014.

[15] C. Choeung, M. L. Kry, and Y. I. Lee, "Robust tracking control of a three-phase charger under unbalanced grid conditions," *Energies*, vol. 11, no. 12, p. 3389, 2018.

[16] C. Choeung, M. Leang Kry, and Y. Il Lee, "Robust tracking control of a three-phase charger under unbalanced grid condition," *IFAC-PapersOnLine*, vol. 51, no. 28, pp. 173–178, 2018.

[17] T.-S. Lee, "Input-output linearization and zero-dynamics control of three-phase AC/DC voltage-source converters," *IEEE Transactions on Power Electronics*, vol. 18, no. 1, pp. 11–22, 2003.

[18] S. K. Kim, D. K. Choi, K. B. Lee, and Y. I. Lee, "Offset-free model predictive control for the power control of three-phase AC/DC converters," *IEEE Transactions on Industrial Electronics*, vol. 62, no. 11, pp. 7114–7126, 2015.

[19] T.-S. Lee, "Lagrangian modeling and passivity based control of three-phase PWM AC/DC voltage source converters," *IEEE Transactions on Industrial Electronics*, vol. 51, no. 4, pp. 892–902, 2014.

[20] S. P. Boyd, L. E. Ghaoui, E. Xiong, and J. Chen, *Linear Matrix Inequalities in System and Control Theory*, SIAM, Philadelphia, PA, USA, 1994.

[21] J. A. Suul, A. Luna, P. Rodriguez, and T. Undeland, "Virtual-flux-based voltage-sensor- less power control for unbalanced grid conditions," *IEEE Transactions on Power Electronics*, vol. 27, no. 9, pp. 4071–4087, 2012.

[22] P. Kanjiya, V. Khadkikar, and M. S. E. Moursi, "Obtaining performance of type-3 phase-locked loop without compromising the benefits of type-2 control system," *IEEE Transactions on Power Electronics*, vol. 33, no. 2, pp. 1788–1796, 2018.